VIP Photocatalysis Very Important Paper

Deutsche Ausgabe: DOI: 10.1002/ange.201605591
Internationale Ausgabe: DOI: 10.1002/anie.201605591

Graphitic Carbon Nitride/Nitrogen-Rich Carbon Nanofibers: Highly Efficient Photocatalytic Hydrogen Evolution without Cocatalysts

*Qing Han, Bing Wang, Jian Gao, and Liangti Qu**

Abstract: *An interconnected framework of mesoporous graphitic-C_3N_4 nanofibers merged with in situ incorporated nitrogen-rich carbon has been prepared. The unique composition and structure of the nanofibers as well as strong coupling between the components endow them with efficient light-harvesting properties, improved charged separation, and a multidimensional electron transport path that enhance the performance of hydrogen production. The as-obtained catalyst exhibits an extremely high hydrogen-evolution rate of 16885 $\mu mol\,h^{-1}\,g^{-1}$, and a remarkable apparent quantum efficiency of 14.3 % at 420 nm without any cocatalysts, which is much higher than most reported g-C_3N_4-based photocatalysts even in the presence of Pt-based cocatalysts.*

Solar-to-chemical energy conversion by photocatalytic hydrogen production from water is considered the cleanest renewable energy source, and has thus attracted considerable attention. The development of efficient photocatalysts is the key objective in photochemical research. Since the seminal work of Fujishima and Honda, where TiO_2 electrodes were used for photocatalytic hydrogen evolution, earth-abundant semiconductors have been extensively investigated as photocatalysts for water splitting.[1] To date, most semiconductor-based photocatalysts demand the utilization of cocatalysts to form surface junctions, thus optimizing light harvesting, improving charge separation and surface catalytic kinetics to achieve efficient photocatalytic activity.[1b–e] However, the widely used cocatalysts usually contain rare and expensive noble metals, which are not suitable for large-scale practical applications. The development of high-performance visible-light-driven photocatalysts that are both stable and cost-efficient nature is required for hydrogen production.

Graphitic carbon nitride (g-C_3N_4) has attracted considerable attention because of its good chemical stability, resistance to photocorrosion, and unique electronic and optical properties that can split water into hydrogen and oxygen under visible light.[2] However, g-C_3N_4 faces low photocatalytic efficiency and relies on surface cocatalysts (e.g., H_2PtCl_6) to reach reasonable activity. An alternative strategy to improve the efficiency of H_2 evolution is to develop g-C_3N_4-based composites where the photogenerated charge separation occurs through the formation of surface junctions.[3] In this regard, graphene could serve as a support matrix to promote the charge transfer and separation generated from g-C_3N_4 because of the high conductivity, intrinsic carrier mobility, and specific surface area of graphene.[4] Accordingly, the composites of g-C_3N_4 with other carbon materials (e.g., multiwalled carbon nanotubes, carbon black, or carbon nanodots) have also been prepared to achieve enhanced photocatalytic activity; in these composites, carbon materials act as a conductive material to transfer the photogenerated electrons or chemical catalysts for H_2O_2 decomposition.[5] Unfortunately, most catalytic systems still depend on the assistance of cocatalysts and their photocatalytic efficiencies need further improvement.

Herein, we report the preparation of an interconnected framework of mesoporous g-C_3N_4 nanofibers merged with in situ incorporated N-rich carbon (g-C_3N_4@C). The strongly coupled binary structure, 3D porous skeleton, and high surface area favor efficient photogenerated charge separation and transfer and also enhance the light-harvesting efficiency. As a result, the g-C_3N_4@C hybrid exhibited an ultrahigh hydrogen evolution rate of 16885 $\mu mol\,h^{-1}\,g^{-1}$ without the assistance of any cocatalysts under $\lambda > 420$ nm irradiation, and an outstanding apparent quantum efficiency of 14.3 % at 420 nm.

The general procedure for the synthesis of 3D g-C_3N_4@C framework is shown in Figure 1 (see the Supporting Information for details). Briefly, the hydrothermally treated dicyandiamide (HTD; Figure 1 a) solution was freeze-dried to form a 3D interconnected network of fiberlike structures (Figure 1 b, and Figure S1). After the absorption of iodine vapour, iodine-loaded HTD induced the oxidation reaction of the pyrrole monomer (Figure 1 c) to form the polypyrrole coating in situ on the HTD nanofibers (HTD-PPY; Figure 1 d), which was confirmed by X-ray diffraction (XRD), FTIR spectroscopy, thermogravimetric analysis (TGA), and Raman spectroscopy (Figure S2 and S3). The obtained HTD-PPY fibers showed features (Figure S4) similar to the original HTD, but with an increased C/N atom ratio from 1.70 to 2.14 and a reduced oxygen content from 24.33 at % to 14.49 at % (Table S1), thus further indicating the effective chemical oxidation polymerization of pyrrole. The subsequent calcination of HTD-PPY resulted in the formation of g-C_3N_4@C (Figure 1 e). PPY was specifically chosen as the carbon source to generate the N-rich carbon (N-carbon) coating layer (Figure S5) along the g-C_3N_4 backbones, which would modulate the nitrogen content in the carbon nitride compound by nitrogen doping. In addition, N-carbon forms close interfacial

[*] Q. Han, B. Wang, J. Gao, Prof. L. Qu
Beijing Key Laboratory of Photoelectronic/Electrophotonic Conversion Materials, Key Laboratory of Cluster Science
Ministry of Education, School of Chemistry
Beijing Institute of Technology
Beijing 100081 (P.R. China)
E-mail: lqu@bit.edu.cn

Supporting information for this article can be found under: http://dx.doi.org/10.1002/anie.201605591.

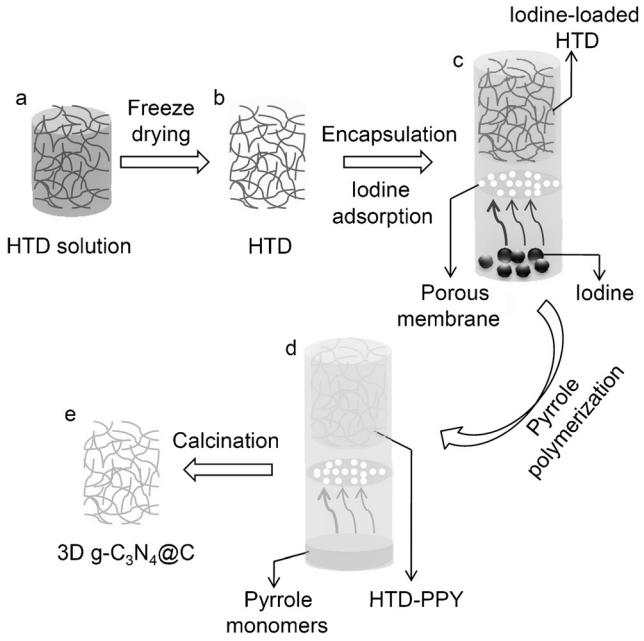

Figure 1. Experimental procedure for fabrication of the 3D g-C_3N_4@C. a) HTD solution; b) freeze-dried HTD; c) iodine-loaded HTD; d) HTD–PPY; e) g-C_3N_4@C.

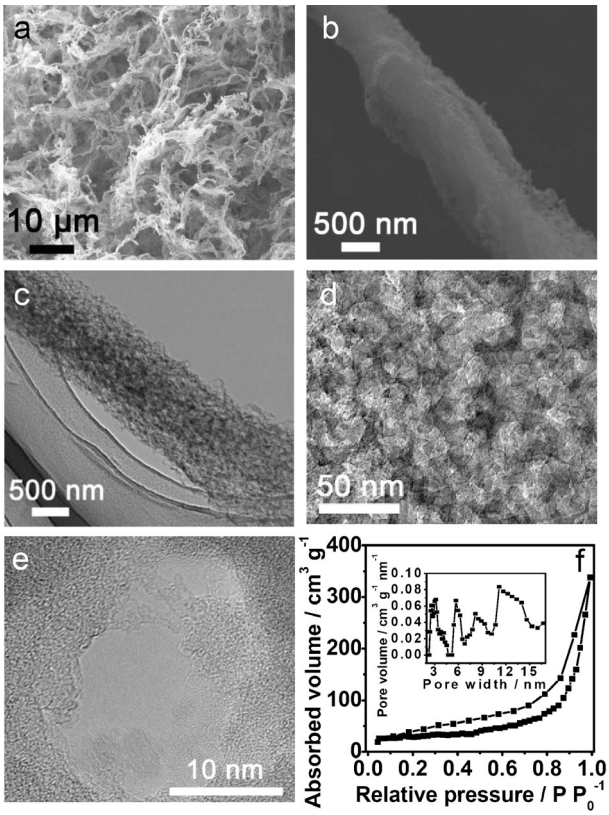

Figure 2. a) Low- and b) high-magnification SEM images of g-C_3N_4@C; c–e) TEM image and the enlarged view of g-C_3N_4@C; f) N_2 adsorption isotherms of g-C_3N_4@C. The inset in (f) is the pore size distribution of g-C_3N_4@C.

contacts more readily, which has an important effect on the photocatalytic performance.[6]

Scanning electron microscopy (SEM) images in Figure 2a,b show that g-C_3N_4@C framework is assembled from cross-linked fibers with diameters of hundreds of nanometers, similar to that of g-C_3N_4 fibers (Figure S6a,b). Transmission electron microscopy (TEM) images show the fibers of g-C_3N_4@C are enriched with mesopores of less than 20 nm (Figure 2c,d). The hydrothermal treatment/vacuum freeze-drying method results in the formation of mesoporous fiber as demonstrated in our previous work.[7a] Compared to g-C_3N_4 (Figure S6d,e), the surface and holes of g-C_3N_4@C feature thin layered structures (Figure 2d,e and Figure S7) associated with the coating of N-carbon (Figure S5a–c). The Brunauer-Emmett–Teller (BET) surface area of g-C_3N_4@C is approximately 372 $m^2 g^{-1}$ (Figure 2f), larger than that of g-C_3N_4 (ca. 330 $m^2 g^{-1}$, Figure S6f). The pore size is mainly less than 20 nm (inset in Figure 2f), consistent with the TEM observations.

The element mappings reveal the coexistent and uniform distribution of C and N element for g-C_3N_4@C (Figure 3a–c). The XPS spectrum of g-C_3N_4@C (Figure 3d) shows the C1s peak at 284.3 eV, N1s at 399 eV, and O1s at 532 eV, similar to g-C_3N_4 (Figure S8a).[7] However, the C/N atomic ratio increases from 0.72 for g-C_3N_4 to 0.86 for g-C_3N_4@C. High-resolution N1s spectra (Figure 3e) shows g-C_3N_4@C consists of 53.8% pyridinic nitrogen (N1, 398.8 eV), 19.1% tertiary nitrogen (N2, 399.7 eV), 16.6% amino functional groups (N3, 401 eV), 6.5% pyrrolic nitrogen (N4, 400.5 eV), and 4% N-graphitic carbon (N5, 397.9 eV),[8] whereas no N4 and N5 signals can be detected in g-C_3N_4 (Figure S8b). The 4% N-graphitic carbon peak could be attributed to the formation of C–N–C bonding,[9] which serves to link N-carbon with g-C_3N_4. The C1s spectrum of g-C_3N_4@C (Figure 3f) exhibits 71.5% N–C=N (C1, 284.9 eV) and 28.5% C–C (C2, 288.5 eV).[2,8] With respect to g-C_3N_4 (Figure S8c), g-C_3N_4@C displays a decrease in the case of N1, N2, and C1, an increase of N3 and C2 (Table S2), which match the energy dispersive X-ray spectrum (EDS) in Figure S9, thus revealing that the effective incorporation of N-carbon in the 3D interconnected g-C_3N_4 network changes the chemical states of C and N species, which is considered important for the photocatalytic activity. The XRD patterns, TGA analysis, FTIR, and Raman spectra of g-C_3N_4@C in comparison with g-C_3N_4, N-carbon, and a physical mixture of g-C_3N_4 and N-carbon (designed as g-C_3N_4/C) shown in Figure S10 further implicate the strong interaction between N-carbon and g-C_3N_4 in g-C_3N_4@C.

The ultraviolet/visible (UV/Vis) absorption of g-C_3N_4@C shows an increase over the whole optical spectrum (Figure 4a) with respect to g-C_3N_4. The corresponding band-gap energy is estimated from the Tauc plot, in which $(F(R)hv)^{1/2}$ is plotted versus the photon energy ($F(R)$ = diffuse absorption coefficient, h = Planck constant and v = light frequency). The obtained band gaps are 2.2 eV for g-C_3N_4@C and 2.7 eV for g-C_3N_4 (inset in Figure 4a). A lower band gap of g-C_3N_4@C is beneficial for efficient absorption of solar light. This effect is also confirmed by the photoluminescence spectra (Figure 4b), where the emission peak of g-C_3N_4@C is red-shifted

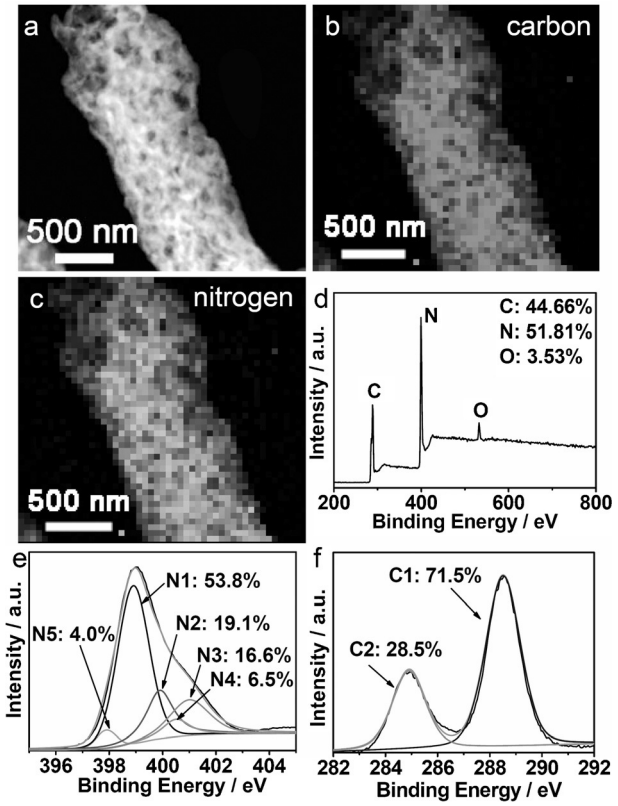

Figure 3. a) HAADF-STEM image and b, c) the corresponding HAADF-STEM-EDS C and N element mapping images of g-C_3N_4@C; d) XPS spectra; e, f) corresponding high-resolution C1s and N1s peak of g-C_3N_4@C.

in comparison to that of g-C_3N_4, in accordance with the narrowed band gap. In addition, the otherwise strong photoluminescence quenching of g-C_3N_4@C suggests that the energetically unfavorable charge recombination is substantially suppressed, thus improving charge separation.[8a–c] In contrast to g-C_3N_4, a smaller peak for g-C_3N_4@C in the Nyquist plot (Figure 4c) indicates that electrons can be easily transferred to the protons in the electrolyte from the conduction band of g-C_3N_4@C. The obvious photocurrent enhancement (Figure 4d) for g-C_3N_4@C suggests an improved charge separation,[8a–c] in agreement with the EIS data. These results confirm the enhanced light-harvesting ability, efficient electron–hole separation, and interfacial charge transfer for the g-C_3N_4@C hybrid. As proposed above, the variation of these properties should be owed to the structural benefits of g-C_3N_4@C because its open-framework construction can create new surface states for charge traps. Simultaneously, the red-shift of the absorption spectrum of g-C_3N_4@C with N-carbon upon N-doping implies that photogenerated electron transfer onto its surfaces for reaction with water molecules is facilitated, which could in turn inhibit the charge recombination and therefore an enhancement of the photocatalytic performance.[10]

The obtained g-C_3N_4@C was tested for H_2 evolution under visible-light irradiation using triethanolamine as sacrificial reagent. As shown in Figure 5a, the H_2 production rate of

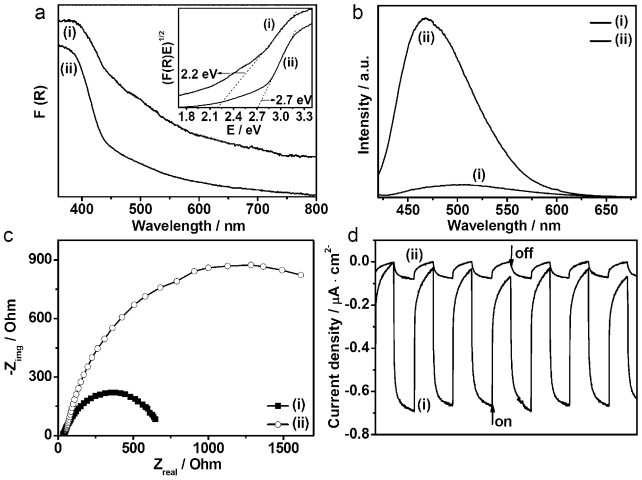

Figure 4. a) UV/Vis diffuse reflectance spectra and band-gap energies (inset) of i) g-C_3N_4@C and ii) g-C_3N_4; b) PL spectra of i) g-C_3N_4@C and ii) g-C_3N_4 (excitation wavelength = 400 nm); c) Electrochemical impedance spectroscopy (EIS) Nyquist plots for i) g-C_3N_4@C and ii) g-C_3N_4 obtained in the dark. d) Transient photocurrents of i) g-C_3N_4@C and ii) g-C_3N_4 ($\lambda > 420$ nm) in 0.2 M Na_2SO_4 aqueous solution (pH 6.8).

g-C_3N_4@C reached 16885 μmol h^{-1} g^{-1}, which is 18.3 times higher than g-C_3N_4 (921 μmol h^{-1} g^{-1}) and arises from the improved electron transfer and enhanced light absorbance. In contrast, the production rate for g-C_3N_4@C was 3.6 times higher than that of Pt/g-C_3N_4 (4665 μmol h^{-1} g^{-1}) and 12.5 times that of the physical mixture of g-C_3N_4/C (1354 μmol h^{-1} g^{-1}), thus indicating that g-C_3N_4@C undergoes fast charge carrier transfer and the incorporated N-carbon could act as a cocatalyst for improved surface reaction kinetics.[8] Furthermore, for Pt/g-C_3N_4@C, the H_2 production rate further increased to 46011 μmol h^{-1} g^{-1}, which is approximately 9.9 times higher than that of Pt/g-C_3N_4 (4665 μmol h^{-1} g^{-1}). Meanwhile, no H_2 was detected for

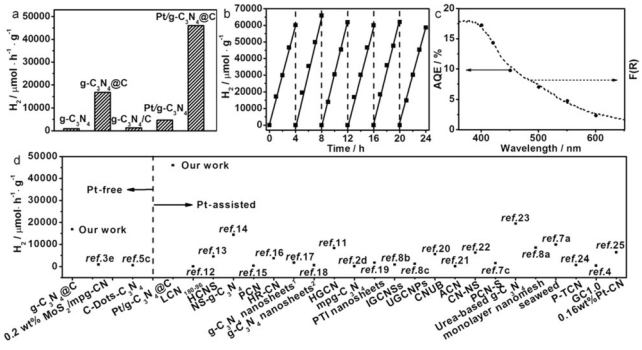

Figure 5. a) Photocatalytic activities of g-C_3N_4, g-C_3N_4@C, g-C_3N_4/C, Pt/g-C_3N_4, and Pt/g-C_3N_4@C (g-C_3N_4, g-C_3N_4@C, and g-C_3N_4/C were tested for hydrogen evolution without Pt cocatalysts; for Pt/g-C_3N_4 and Pt/g-C_3N_4@C the hydrogen evolution was measured with the assistance of Pt cocatalysts $\lambda > 420$ nm); b) stable hydrogen evolution by g-C_3N_4@C without cocatalyst ($\lambda > 420$ nm); c) wavelength dependence of H_2 evolution rate of g-C_3N_4@C without cocatalyst; d) hydrogen evolution rate for g-C_3N_4@C in comparison with other g-C_3N_4-based catalysts. The specific test conditions are given in Table S3.

N-carbon alone under identical experimental conditions, thus implying the N-carbon itself without g-C_3N_4 is not active for photocatalytic H_2 production. The g-C_3N_4@C was reused over six cycles without noticeable deactivation of its hydrogen photoproduction (Figure 5b), thus indicating that the high activity is reproducible. Wavelength-dependent H_2 evolution reveals the catalytic activity of g-C_3N_4@C matches its optical absorption spectrum, thus suggesting that the H_2 production is primarily driven by photoinduced electrons in this carbon nitride polymer (Figure 5c). The calculated apparent quantum efficiency (AQE) of g-C_3N_4@C is 14.3% at 420 nm. To the best of our knowledge, thus is the highest reported value for g-C_3N_4-based photocatalysts without the assistance of cocatalysts (Table S3). The H_2 production rate of g-C_3N_4@C is significantly higher than that of most g-C_3N_4-based photocatalysts reported previously (Figure 5d and Table S3). However, a further increase of N-carbon coating led to dramatically decreased catalytic performance (Table S4 and Figure S11–14), probably because the excess of black N-carbon resulted in the shielding of the active sites on the catalyst surface and reduced the light penetration depth in the reaction solution.[1d]

On the basis of the above results, a tentative mechanism for the catalytic system is proposed (see Figure S15). Upon irradiation, excited electrons are generated in g-C_3N_4 and move from the valence to the conduction bands, and then are transferred to carbon or nitrogen atoms on N-carbon. Subsequently, the captured electrons react with water to generate H_2. Although the CB edge of g-C_3N_4 is more negative than the reduction potential of H_2/H_2O (Figure S16), the H_2 production rate of g-C_3N_4 is much lower than that of g-C_3N_4@C simply because of the rapid recombination of photogenerated electrons and holes. When N-carbon is introduced into g-C_3N_4, it behaves as an electron acceptor and transporter to separate the electron–hole pairs. In addition, the photocatalytic reactions could occur on the surface of both g-C_3N_4 catalysts and N-carbon, thus increasing the available reaction space.

In summary, we have prepared mesoporous g-C_3N_4 nanofibers incorporated with N-rich carbon. The hierarchical architecture of the nanostructure and strong coupling effect between g-C_3N_4 and N-carbon in the hybrid favor the light harvesting, efficient charge separation, rapid carrier transfer, and utilization of active adsorption sites, result in an ultrahigh photocatalytic activity without any cocatalysts. This work provides a simple method for designing intimate and effective interfacial junctions for optoelectronic, photocatalytic and photoelectrocatalytic applications.

Acknowledgements

This work was supported by NSFC (No. 21325415), National Basic Research Program of China (2011CB013000), and Beijing Natural Science Foundation (2152028).

Keywords: charge separation · graphitic carbon nitride · hydrogen evolution · nitrogen-rich carbon · photocatalysis

How to cite: *Angew. Chem. Int. Ed.* **2016**, *55*, 10849–10853
Angew. Chem. **2016**, *128*, 11007–11011

[1] a) A. Fujishima, K. Honda, *Nature* **1972**, *238*, 37–38; b) A. Kudo, Y. Miseki, *Chem. Soc. Rev.* **2009**, *38*, 253–278; c) J. Hensel, G. Wang, Y. Li, J. Z. Zhang, *Nano Lett.* **2010**, *10*, 478–483; d) Q. Li, B. D. Guo, J. G. Yu, J. R. Ran, B. H. Zhang, H. J. Yan, J. R. Gong, *J. Am. Chem. Soc.* **2011**, *133*, 10878–10884; e) T. C. Johnson, D. J. Morris, M. Wills, *Chem. Soc. Rev.* **2010**, *39*, 81–88.

[2] a) X. C. Wang, K. Maeda, A. Thomas, K. Takanabe, G. Xin, J. M. Carlsson, K. Domen, M. Antonietti, *Nat. Mater.* **2008**, *8*, 76–80; b) Y. Zheng, J. Liu, J. Liang, M. Jaroniec, S. Z. Qiao, *Energy Environ. Sci.* **2012**, *5*, 6717–6731; c) Y. Wang, X. Wang, M. Antonietti, *Angew. Chem. Int. Ed.* **2012**, *51*, 68–89; *Angew. Chem.* **2012**, *124*, 70–92; d) X. Wang, K. Maeda, X. Chen, K. Takanbe, K. Domen, Y. Hou, X. Fu, M. Antonietti, *J. Am. Chem. Soc.* **2009**, *131*, 1680–1681.

[3] a) X. H. Li, J. S. Chen, X. C. Wang, J. H. Sun, M. Antonietti, *J. Am. Chem. Soc.* **2011**, *133*, 8074–8077; b) J. Zhang, M. Zhang, R. Q. Sun, X. Wang, *Angew. Chem. Int. Ed.* **2012**, *51*, 10145–10149; *Angew. Chem.* **2012**, *124*, 10292–10296; c) Y. Wang, R. Shi, J. Lin, Y. Zhu, *Energy Environ. Sci.* **2011**, *4*, 2922–2929; d) F. Meng, J. Li, S. K. Cushing, M. Zhi, N. Wu, *J. Am. Chem. Soc.* **2013**, *135*, 10286–10289; e) Y. D. Hou, A. B. Laursen, J. S. Zhang, G. G. Zhang, Y. S. Zhu, X. C. Wang, S. Dahl, I. Chorkendorff, *Angew. Chem. Int. Ed.* **2013**, *52*, 3621–3625; *Angew. Chem.* **2013**, *125*, 3709–3713; f) X. H. Li, M. Antonietti, *Chem. Soc. Rev.* **2013**, *42*, 6593–6604; g) S. W. Cao, J. X. Low, J. G. Yu, M. Jaroniec, *Adv. Mater.* **2015**, *27*, 2150–2176.

[4] Q. J. Xiang, J. G. Yu, M. Jaroniec, *J. Phys. Chem. C* **2011**, *115*, 7355–7363.

[5] a) Y. Chen, J. Li, Z. Hong, B. Shen, B. Lin, B. Gao, *Phys. Chem. Chem. Phys.* **2014**, *16*, 8106–8113; b) Z. Wu, H. Gao, S. Yan, Z. Zou, *Dalton Trans.* **2014**, *43*, 12013–12017; c) J. Liu, Y. Liu, N. Y. Liu, Y. Z. Han, X. Zhang, H. Huang, Y. Lifshitz, S. T. Lee, J. Zhong, Z. H. Kang, *Science* **2015**, *347*, 970–974.

[6] D. W. Chang, J. B. Baek, *Chem. Asian J.* **2016**, *11*, 1125–1137.

[7] a) Q. Han, B. Wang, Y. Zhao, C. G. Hu, L. T. Qu, *Angew. Chem. Int. Ed.* **2015**, *54*, 11433–11437; *Angew. Chem.* **2015**, *127*, 11595–11599; b) X. Zhang, X. Xie, H. Wang, J. Zhang, B. Pan, Y. Xie, *J. Am. Chem. Soc.* **2013**, *135*, 18–21; c) J. R. Ran, T. Y. Ma, G. P. Gao, X. W. Du, S. Z. Qiao, *Energy Environ. Sci.* **2015**, *8*, 3708–3717.

[8] a) Q. Han, B. Wang, J. Gao, Z. H. Cheng, Y. Zhao, Z. P. Zhang, L. T. Qu, *ACS Nano* **2016**, *10*, 2745–2751; b) Q. Han, C. G. Hu, F. Zhao, Z. P. Zhang, N. Chen, L. T. Qu, *J. Mater. Chem. A* **2015**, *3*, 4612–4619; c) Q. Han, F. Zhao, C. G. Hu, L. X. Lv, Z. P. Zhang, N. Chen, L. T. Qu, *Nano Res.* **2015**, *8*, 1718–1728; d) Y. Zhao, F. Zhao, X. P. Wang, C. Y. Xu, Z. P. Zhang, G. Q. Shi, L. T. Qu, *Angew. Chem. Int. Ed.* **2014**, *53*, 13934–13939; *Angew. Chem.* **2014**, *126*, 14154–14159; e) D. S. Geng, Y. Chen, Y. G. Chen, Y. L. Li, R. Y. Li, X. L. Sun, S. Y. Ye, S. Knights, *Energy Environ. Sci.* **2011**, *4*, 760–764; f) W. Ding, Z. D. Wei, S. G. Chen, X. Q. Qi, T. Yang, J. S. Hu, D. Wang, L. J. Wan, S. F. Alvi, L. Li, *Angew. Chem. Int. Ed.* **2013**, *52*, 11755–11759; *Angew. Chem.* **2013**, *125*, 11971–11975.

[9] Y. Hou, Z. H. Wen, S. M. Cui, X. L. Feng, J. H. Chen, *Nano. Lett.* **2016**, *16*, 2268–2277.

[10] G. H. Dong, K. Zhao, L. Z. Zhang, *Chem. Commun.* **2012**, *48*, 6178–6180.

[11] Q. H. Liang, Z. Li, Z. H. Huang, F. Y. Kang, Q. H. Yang, *Adv. Funct. Mater.* **2015**, *25*, 6885–6892.

[12] Y. J. Cui, Z. X. Ding, X. Z. Fu, X. C. Wang, *Angew. Chem. Int. Ed.* **2012**, *51*, 11814–11818; *Angew. Chem.* **2012**, *124*, 11984–11988.

[13] J. H. Sun, J. S. Zhang, M. W. Zhang, M. Antonietti, X. Z. Fu, X. C. Wang, *Nat. Commun.* **2012**, *3*, 1139 – 1146.
[14] J. S. Zhang, M. W. Zhang, C. Yang, X. C. Wang, *Adv. Mater.* **2014**, *26*, 4121 – 4126.
[15] J. Hong, S. Yin, Y. Pan, J. Han, T. Zhou, R. Xu, *Nanoscale* **2014**, *6*, 14984 – 14990.
[16] Y. Zheng, L. H. Lin, X. J. Ye, F. S. Guo, X. C. Wang, *Angew. Chem. Int. Ed.* **2014**, *53*, 11926 – 11930; *Angew. Chem.* **2014**, *126*, 12120 – 12124.
[17] S. B. Yang, Y. J. Gong, J. S. Zhang, L. Zhan, L. L. Ma, Z. Y. Fang, R. Vajtai, X. C. Wang, P. M. Ajayan, *Adv. Mater.* **2013**, *25*, 2452 – 2457.
[18] P. Niu, L. Zhang, G. Liu, H. M. Cheng, *Adv. Funct. Mater.* **2012**, *22*, 4763 – 4770.
[19] K. Schwinghammer, M. B. Mesch, V. Duppel, C. Ziegler, J. Senker, B. V. Lotsch, *J. Am. Chem. Soc.* **2014**, *136*, 1730 – 1733.
[20] Z. Z. Lin, X. C. Wang, *Angew. Chem. Int. Ed.* **2013**, *52*, 1735 – 1738; *Angew. Chem.* **2013**, *125*, 1779 – 1782.
[21] Y. Kang, Y. Yang, L. Yin, X. Kang, G. Liu, H. M. Cheng, *Adv. Mater.* **2015**, *27*, 4572 – 4577.
[22] G. G. Liu, T. Wang, H. B. Zhang, X. G. Meng, D. Hao, K. Chang, P. Li, T. Kako, J. H. Ye, *Angew. Chem. Int. Ed.* **2015**, *54*, 13561 – 13565; *Angew. Chem.* **2015**, *127*, 13765 – 13769.
[23] D. J. Martin, K. P. Qiu, S. A. Shevlin, A. D. Handoko, X. W. Chen, Z. X. Guo, J. W. Tang, *Angew. Chem. Int. Ed.* **2014**, *53*, 9240 – 9245; *Angew. Chem.* **2014**, *126*, 9394 – 9399.
[24] S. Guo, Z. P. Deng, M. X. Li, B. J. Jiang, C. G. Tian, Q. J. Pan, H. G. Fu, *Angew. Chem. Int. Ed.* **2016**, *55*, 1830 – 1834; *Angew. Chem.* **2016**, *128*, 1862 – 1866.
[25] X. G. Li, W. T. Bi, L. Zhang, S. Tao, W. S. Chu, Q. Zhang, Y. Luo, C. Z. Wu, Y. Xie, *Adv. Mater.* **2016**, *28*, 2427 – 2431.

Received: June 8, 2016
Revised: July 7, 2016
Published online: July 28, 2016

